CrossMark

ORIGINAL PAPER

A new prediction model for rock slope failure time: a case study in West Open-Pit mine, Fushun, China

Lei Nie[1] · Zechuang Li[1] · Yan Lv[1] · Hongfei Wang[1]

Abstract Establishing an accurate method for predicting the failure times of rock slopes subject to creep deformation is challenging, but at the same time crucial for preventing damage to properties and loss of life. In this paper, the Medium–short Term Prediction of Landslide by Polynomial (MsTPLP) model is proposed based on the Levenberg–Marquardt (LM) algorithm. The West Open-Pit mine in Fushun, NE China is currently the largest open-pit coal mine in Asia. The landslide on the southern slope of the West Open-Pit mine was selected as the study case. Global Positioning System (GPS) monitoring is employed in landslide displacement monitoring. Based on the analysis process of the MsTPLP model, the displacement time series derived from GPS monitoring points is selected as the input. The model parameters of the MsTPLP model are obtained using the Levenberg–Marquardt (LM) algorithm. The predicted failure time of a landslide, which is the output, can be determined according to the prediction criteria of the model. The prediction results show that the MsTPLP model can provide accurate landslide displacement predictions (correlation coefficient $R^2 > 0.98$ and average relative error ARE < 17 %). The forecasting results of the landslide show that the estimated failure time is Mar 5, 2014. Based on field investigation and displacement analysis, the landslide on the southern slope of the West Open-Pit mine occurred on Mar 9, 2014. The predicted and actual failure times are significantly close, demonstrating the potential of the new method in landslide prediction.

Keywords Landslide · Failure prediction · West Open-Pit mine · Levenberg–Marquardt algorithm

Introduction

Landslides in Asian countries cause major socio-economic disruptions, extensive property damage, and casualties (Du et al. 2013). In China alone, 9849 landslides that occurred in 2013 accounted for 63.9 % of the total number of geological disasters, and the main contributing factors were rain, earthquakes, and cut slopes (China Geological Environmental Monitoring Institute 2014; Zhang et al. 2015). Landslide failure time prediction may be an effective method to avoid property damage and casualties (Nie et al. 2013; Rose and Hungr 2007; Wang and Nie 2010).

Landslides are complex geological phenomena (Radbruch-Hall and Varnes 1976; Griffiths 1999; Sidle and Ochiai 2006). Landslide prediction is a difficult task that requires a thorough study of past activities and a complete range of investigative methods to determine change conditions (Chen et al. 2015). Landslide displacement monitoring data is vital in analyzing the dynamics of landslide movement, which is a key factor in the prediction of failure time (Liu et al. 2014; Mazzanti et al. 2015). In the last decade, owing to the development of the Global Positioning System (GPS) technique, more accurate landslide displacement data have been obtained (Lian et al. 2015).

The time prediction of a landslide failure remains a universal challenge at present because landslides are often characterized by complex geometries and combinations of heterogeneous materials with different features (Qin et al.

✉ Zechuang Li
zechuang.li@foxmail.com

Lei Nie
nielei@jlu.edu.cn

[1] College of Construction Engineering, Jilin University, Changchun 130026, China

🌲 Springer

2001; Sättele et al. 2015; Cai et al. 2015). The models for landslide failure time prediction can be roughly classified into three types: deterministic, statistical, and nonlinear (Li et al. 2012). A summary of the different methods proposed in the literature can be found in Federico et al. (2012). However, these methods all have some limitations. Although the evolution of an unstable slope demonstrates individuality, such as oscillation or step transition development, certain types of landslides show some common prominent features during their deformation evolution (Xu et al. 2008). These features have not been discussed in detail in most existing studies. Therefore, research should be confined to slopes that have certain common features. Considerable research on the failure mechanism of rock slopes whose potential sliding surface dips more steeply than the slope surface has been undertaken (Huang et al. 2002; Huang 2012). A rocky slope deforms generally over a long period of time until failure, and the deformation shows typical creeping characteristics, a phenomenon known as "slope creep" (Terzaghi 1950; Haefeli 1953). Such slopes that display a progressive increase in deformation rate a few days before the failure are commonly denoted by "creep slopes" (Xu and Zeng 2009; Agliardi et al. 2010; Xu et al. 2011). The plot of these displacement monitoring data shows that the movements exhibit a generally nonlinear asymptotic trend. In this study, the kinematic features of landslides are studied, and a new approach to predicting the failure time of landslides is proposed.

In this paper, based on data of landslide deformation monitoring, a new model called Medium–short Term Prediction of Landslides by Polynomial model (MsTPLP model) is proposed for prediction. In this model, cumulative displacement and monitoring time are selected as inputs. The MsTPLP model parameters are obtained using the Levenberg–Marquardt (LM) algorithm. The prediction curve shape is constantly adjusted to adapt to the evolution process of the landslide. The landslide failure time is predicted as output with the use of the prediction criteria. The West Open-Pit mine in western Fushun, Liaoning Province, NE China is a large deep-sunken open-pit coal mine, which is located in the coordinate system UTM zone 51T (Fig. 1). The landslide on the southern slope of the West Open-Pit Mine was selected as a study case to validate the feasibility of the proposed method. The MsTPLP model was applied to predict the failure time with the use the measured displacement time series derived from the GPS. Three evaluation parameters were calculated, and the difference between the actual and the predicted failure times was determined to assess the correctness and quality of the result. Our model can be used for landslide risk reduction to prevent property damage and loss of lives caused by landslides.

Methodology formulation

The MsTPLP Model

The curve of landslide displacement versus time represents the landslide evolution process, which develops in time through several stages (Leroueil et al. 1996). The MsTPLP model is based on a known evolution process to predict the future evolution process and estimate the failure time of the landslide. The model is based on a large number of landslide cases subject to creep deformation (Xu et al. 2008; Xu and Zeng 2009). As reviewed by Skempton and Hutchinson (1969), the history of a mass movement comprises prefailure deformations, failure itself, and post-failure displacements (Hungr et al. 2014). The landslide pre-failure evolution process, from initial deformation to failure, can be described in three stages: primary stage, secondary
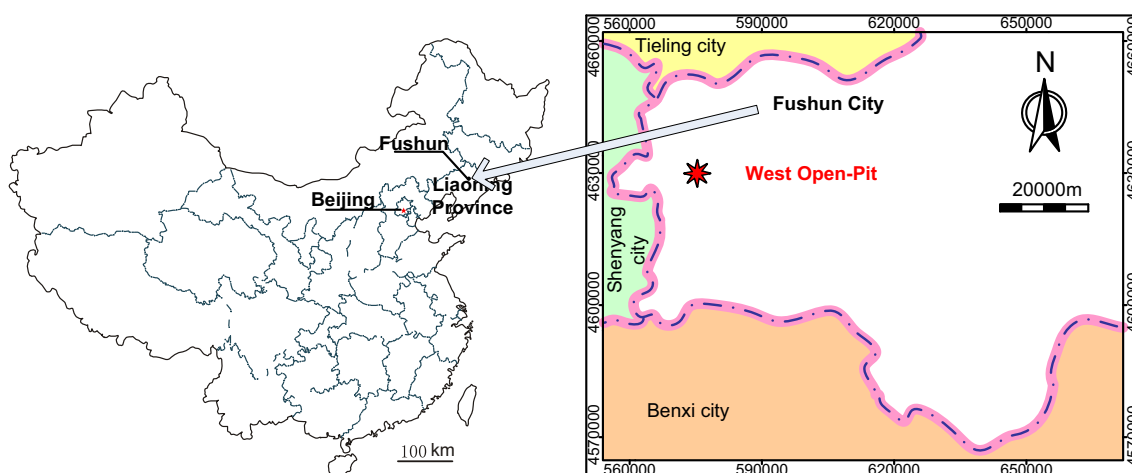

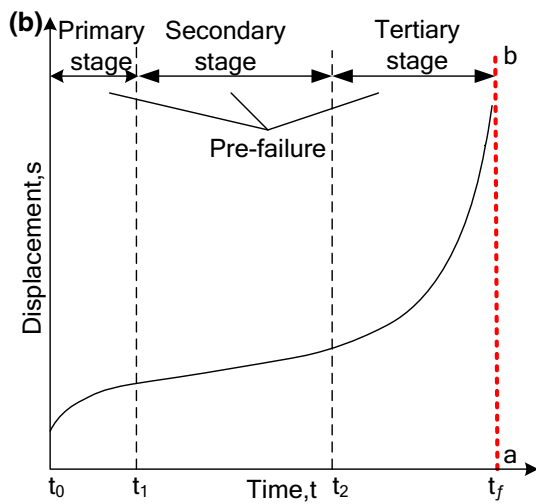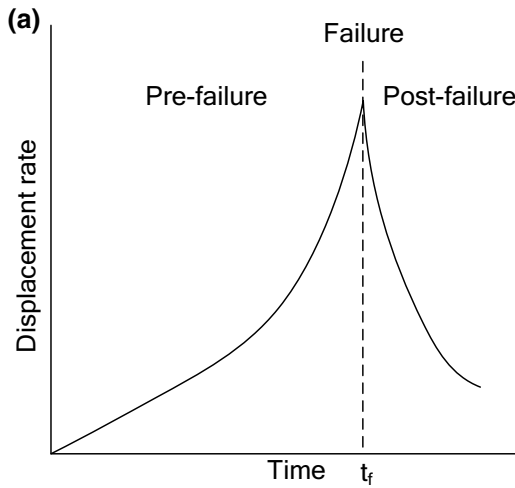**Fig. 1** Location map of the study area mentioned in the paper

(a)

(b)

Fig. 2 a Potential stages in a landslide. **b** Scheme of typical three stages of the landslide pre-failure evolution process

Fig. 3 Predicted landslide displacement versus time according to the MsTPLP model

stage, and tertiary stage with similar features to the creep curve of rock and soil masses (Saito 1969; Crosta and Agliardi 2003; Xu et al. 2011). In the tertiary stage the displacement versus time curve tends to infinity over a short period of time indicating that landslide failure would happen before this point. The vertical asymptotic line ab in Fig. 2 corresponds to the failure time of the landslide.

In this paper, we present the MsTPLP model for the medium–short term prediction of landslides to predict landslide failure time. The proposed prediction model is expressed in Eq. 1:

$$S = \frac{p_1 + p_2 t + p_3 t^2}{p_0 - t} - \frac{p_1}{p_0} \qquad (1)$$

where t is the monitoring time, S is the displacement, p_0, p_1, p_2, and p_3 are undetermined parameters. p_0 represents the failure time of the landslide, $\frac{p_1 + p_0 p_2}{p_0^2}$ represents the initial
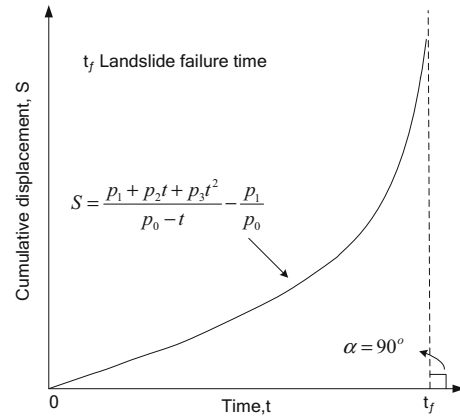
speed, $\frac{2p_1 + 2p_0 p_2 + 2p_0^2 p_3}{p_0^3}$ represents the initial acceleration. The larger value of p_0, p_1 and p_2, the more rapidly the displacement curve approaches the asymptote. In other words, the time required for the failure of the landslide will be shorter.

When the predicted MsTPLP curve intersects the time axis at coordinates (0, 0), i.e., the origin value is zero, the initial displacement of the landslide is zero. The function of the MsTPLP model is a monotonically increasing function (Fig. 3). And the model in the vertical axis direction with convergence shows a point where $\Delta t \to 0$ and $\Delta S \to \infty$, indicating a vertical asymptote. When landslides are in the tertiary stage, the predicted curve of the MsTPLP model is significantly similar to the landslide displacement–time scatter diagram. The first derivative of the predicted curve (the deformation rate function) increases monotonically; when the landslide is in the tertiary stage, the deformation rate increases nonlinearly with time. These indicate that the MsTPLP model can perform well in prediction of landslides. Figure 4 describe the analysis process of the MsTPLP model in a flowchart form.

Model parameters determined by LM algorithm

The monitoring data $(t_i, S_i)(i = 1, 2, \ldots, m)$ is selected as input, where t_i is the monitoring time (days), S_i is the measured displacement value (cm), and m is the number of measured nodes. The model parameters p_0, p_1, p_2, p_3 will vary with changes in the monitoring data. A search for optimal parameters in the model plays a crucial role. The Levenberg–Marquardt (LM) algorithm is introduced to determine the optimal parameters p_0, p_1, p_2, and p_3 of the model, which minimizes the sum of the squared error functions and produces a digital solution to the mathematical problem (Levenberg 1944; Marquardt 1963; Lourakis 2005).
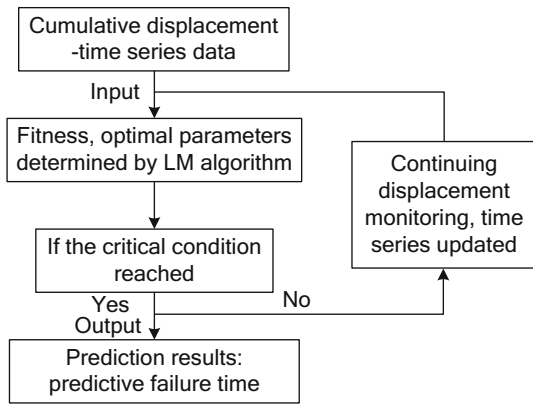
Fig. 4 Analysis flowchart of the MsTPLP model

The error e_i, error volume vector $e(p)$, and the error index function $E(p)$ can be described by

$$E(p) = \frac{1}{2}\sum_{i=1}^{m} e_i^2(p) = \frac{1}{2}\sum_{i=1}^{m}(S(p) - S_i)^2$$
$$= \frac{1}{2}\sum_{i=1}^{m}\left(\frac{p_1 + p_2 t_i + p_3 t_i^2}{p_0 - t_i} - \frac{p_1}{p_0} - S_i\right)^2 \quad (2)$$

where S is the predicted displacement value.

The initial parameters p_0^0, p_1^0, p_2^0, and p_3^0 are provided (see below) and the method seeks the parameters p_0, p_1, p_2, and p_3 that best satisfy the functional relation $\min E(p)$, Eq. 3, i.e., that minimize the squared distance between the predicted value and the measured value:

$$\min E(p) = \min \sum_{i=1}^{m} e_i^2(p)$$
$$= \min \sum_{i=1}^{m}[S_i - S(t_i; p_0, p_1, p_2, p_3)]^2 \cdot i$$
$$= 1, 2\dots, m \quad (3)$$

The numerical form of the LM algorithm is:

$$p^{k+1} = p^k + \Delta p \quad (4)$$

$$(J(p^k)^T J(p^k) + \lambda I)\Delta p = -J(p^k)^T e(p^k) \cdot k = 1, 2\dots, n \quad (5)$$

where k represents the iterations, I is the unit matrix, λ is the damping term, n is the maximum iterations (chosen by the user), and $J(p)$ is the Jacobian matrix

$$J(p) = J(p_0, p_1, p_2, p_3) = \begin{bmatrix} \frac{\partial e_1}{\partial p_0} & \frac{\partial e_1}{\partial p_1} & \frac{\partial e_1}{\partial p_2} & \frac{\partial e_1}{\partial p_3} \\ \frac{\partial e_2}{\partial p_0} & \frac{\partial e_2}{\partial p_1} & \frac{\partial e_2}{\partial p_2} & \frac{\partial e_2}{\partial p_3} \\ \vdots & \vdots & \vdots & \vdots \\ \frac{\partial e_m}{\partial p_0} & \frac{\partial e_m}{\partial p_1} & \frac{\partial e_m}{\partial p_2} & \frac{\partial e_m}{\partial p_3} \end{bmatrix} \quad (6)$$

where

$$J_{i,1} = \frac{\partial e_i}{\partial p_0} = \frac{p_1}{p_0^2} - \frac{p_3 t_i^2 + p_2 t_i + p_1}{(p_0 - t_i)^2} \quad (7)$$

$$J_{i,2} = \frac{\partial e_i}{\partial p_1} = \frac{1}{p_0 - t_i} - \frac{1}{p_0} \quad (8)$$

$$J_{i,3} = \frac{\partial e_i}{\partial p_2} = \frac{t_i}{p_0 - t_i} \quad (9)$$

$$J_{i,4} = \frac{\partial e_i}{\partial p_3} = \frac{t_i^2}{p_0 - t_i} \quad (10)$$

The initial estimation of the parameters p_0^0, p_1^0, p_2^0, and p_3^0, the error threshold ε and the maximum number of iterations n are set by the user. The four parameters p_0, p_1, p_2, and p_3 are calculated by the LM algorithm to nonlinear iterative optimization. The LM algorithm terminates when at least one of the two criteria for the error sum of the squares $E(p) \leq \varepsilon$ and the iterations $k \geq n$ is met. The resulting parameter $p(p_0, p_1, p_2, p_3)$ is accepted.

Prediction criteria

When the cumulative displacement is plotted versus time, the displacement tends to increase asymptotically toward failure after the slope deformation enters the tertiary stage. The time when the gradient of the cumulative displacement tends to infinity is the time of failure. Failure is assumed to occur when the tangential angle α ($\alpha = \arctan(\mathrm{d}S/\mathrm{d}t)$) between the tangent of the displacement–time curve and the time axis is 90°. A trend line (i.e., predicted displacement–time curve) fitting the values of the cumulative displacement versus time based on Eq. 1 can be obtained by the LM algorithm. When the tangential angle of the MsTPLP predicted displacement–time curve is 90°, the tangent corresponding to the tangential angle is a vertical asymptotic line of the predicted curve. The time corresponding to the projection of this tangential on the abscissa (time axis) is the predicted failure time as shown in Fig. 2b.

A trend-line (i.e., predicted displacement–time curve) fit through values of cumulative displacement versus time based on the Eq. 1 can be obtained by the LM algorithm.

Based on the analysis of landslide cases, when the tangential angle of the measured displacement curve reaches 82°, the predicted failure time by the MsTPLP model is reliable and reasonable. Therefore, when the tangential angle of the cumulative displacement curve reaches 82°, the output of the MsTPLP model is the predicted failure time. This value is defined as the critical condition of the MsTPLP model. Between the interference of external factors and measurement errors, the tangential angle of measured displacement tends to fluctuate in the tertiary stage. It is hard to judge whether the tangential angle reach

82°. Therefore, it is imperative to calculate a tangential angle of a short period of time, which can be obtained by:

$$\alpha = \arctan\left(\frac{S_j - S_{j-l}}{l}\right), \tag{11}$$

where S_j is the measured displacement, and l is a short monitoring period of time (7 days generally chosen).

Model evaluation

To quantify the performance of the MsTPLP model for predicting landslides, three evaluation parameters for the variance between the measured values and predicated values were calculated: the correlation coefficient (R^2), the relative error (RE), and the average relative error (ARE). The equations for calculating these coefficients are

$$R^2 = \frac{\left[\sum_{i=1}^{m}(S - \overline{S})\sum_{i=1}^{m}(S_i - \overline{S_i})\right]^2}{\sum_{i=1}^{m}(S - \overline{S})^2 \sum_{i=1}^{m}(S_i - \overline{S_i})^2} \tag{12}$$

$$\text{RE} = \frac{|S_i - S|}{S_i} \tag{13}$$

$$\text{ARE} = \frac{1}{m}\sum_{i=0}^{m}\frac{|S_i - S|}{S_i} \tag{14}$$

where S_i is the measured value, $\overline{S_i}$ is the average measured value, S is the predicted value, $\overline{S}$ is the average predicted value, and m is the measured node number. The values of R^2, RE, and ARE range from 0 to 1. R^2 assesses the fit between the predicted values and the measured values; the higher the value of R^2, the better the fit between the measured and predicted values. Additionally, RE indicates the estimation error and ARE indicates the average estimation error during the entire monitoring period. The smaller the values of RE and ARE, the smaller the prediction errors.

Moreover, the complete displacement rate–time curve of a landslide is divided into pre-failure and post-failure regions according to the peak rate. The monitoring time corresponding to the peak rate is the failure time. As shown in Fig. 2a. This parameter is another key tool to validate the methodology.

Application of the methodology: the landslide prediction

Geological conditions and deformation characteristics

The West Open-Pit mine is a large open-pit coal mine located in western Fushun, Liaoning Province, NE China, with the Qiantai Mountain to the south. Coal extraction began in 1901 and the site has a long mining history of more than 100 years. The West Open-Pit mine is the biggest pit in Asia (Johnson 1990). Its length from east to west is 6.6 km and it has a width of 2.2 km from north to south with a depth of approximately 420 m (Zhou et al. 2011). The landslide is situated on the southern slope of the West Open-Pit mine, which is the largest landslide that have occurred in Asian countries, 1200–1500 m long in the north–south direction, 3100 m wide in the east–west direction, with an estimated volume of 0.1 billion cubic meters (Nie et al. 2015).

The annual average rainfall in the study area is 740–790 mm and is unevenly distributed throughout the year, with higher concentrations in the rainy season (July to September). The rainy season rainfall is about 75 % of the annual rainfall.

The mining area has an F_2 fault in the east–west direction and an F_5 fault in the northwest-southeast direction. The F_2 fault is a normal fault approximately 3 km long, with an east–west strike direction, dipping north with a dip angle of 80°. The F_5 fault is approximately 1700 m long, with a strike direction of S35°E, a dip direction of S55°W and a dip angle of 36°. It is a tension-torsional normal fault. Many joints have also developed in the mining area. The mining strip rock mass forms the bottom of the open-pit and cuts the foot of the slope.

The geological structure of the landslide has been obtained by means of an intense geological and geomorphological assessment, which has included mapping of the surficial exposures, geophysical surveys and drilling. The southern slope of the West Open-Pit mine dips to the north, with an overall slope angle of approximately 19°–27°. The foot of the slope is located at the bottom of the West Open-Pit mine with an elevation between −270 and −330 m while the head has an elevation between +100 and +205 m (Fig. 5). The height of the slope is 400–500 m. The outcrop in the southern slope consists mainly of Mesozoic volcanic tuff, basalts, and Archaean granitic gneiss (Wu et al. 2000; Zhang 2009). Some miscellaneous fill in the main body was observed at the slope surface. The upper tuff was weathered to clay bearing rocks. The basalt layer dips NNW to 315°–356° at an angle of 23°–48°. The upper part of basalts is relatively intact. There is some weak interlayer in the middle and lower part of basalts and the angular unconformity between basalts and granitic gneiss. The dip angle of the weak interlayer is approximately 29° and the granitic gneiss dips to 320°–323° with an angle of 71°–75°. A critical potential sliding surface is found and shown in Section 1-1′ (Fig. 6). The dip angle of the sliding surface is slightly larger than the slope angle. The upper sliding surface is located in the weak interlayer and the outcrop of the sliding surface is beneath the foot of the slope. Behavior of the sliding mass is controlled by this
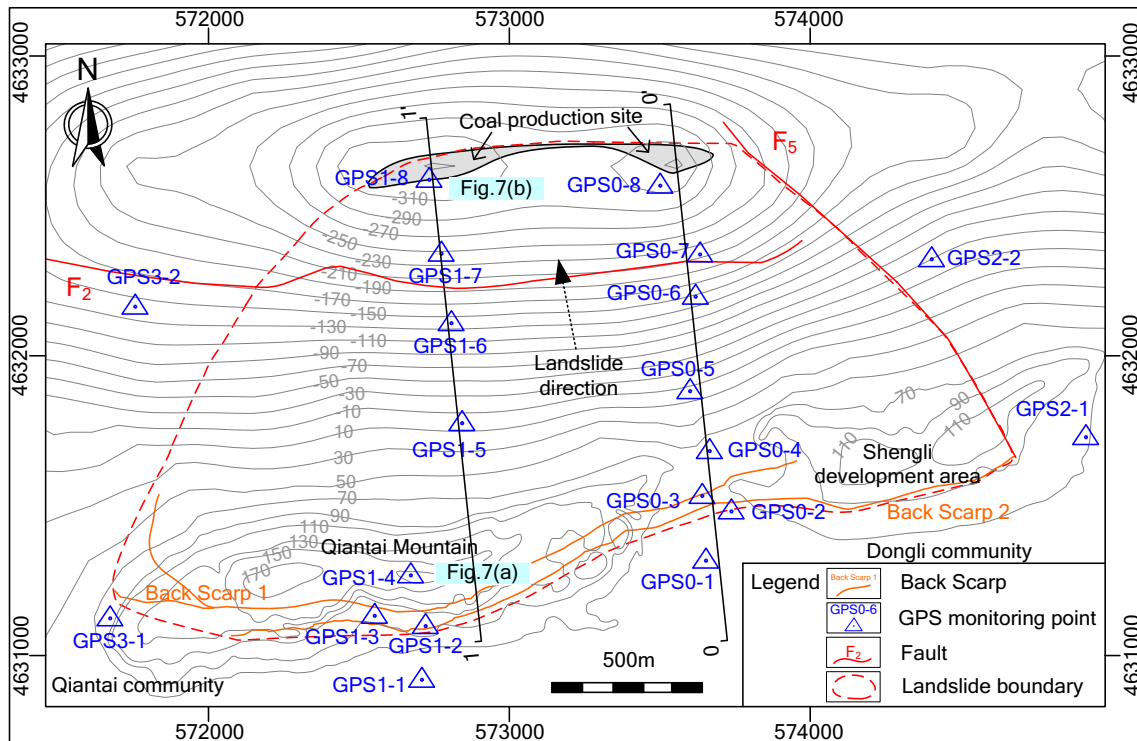
Fig. 5 Topographical map of the landslide, with the distribution of GPS
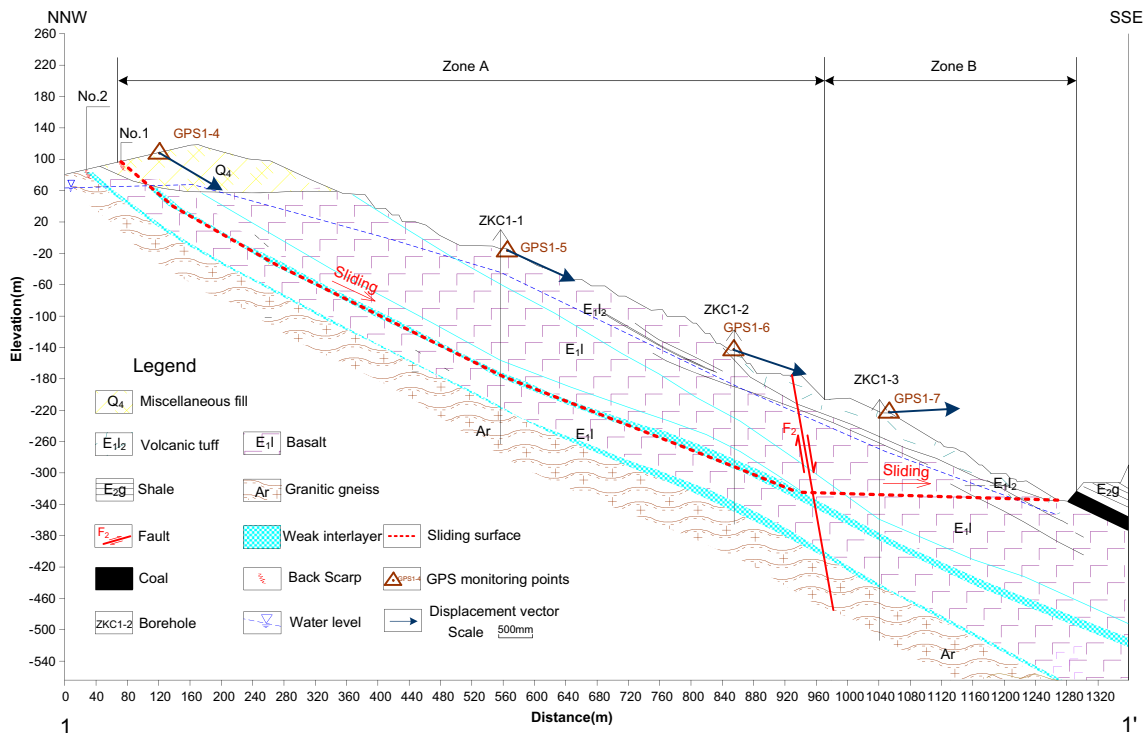

Fig. 6 Geological Section 1–1′ of the landslide (the location of the profile appears in Fig. 5)

weak interlayer's engineering properties. According to the different deformation characteristics, the slope can be divided into two parts: the sliding part in the upper head and middle of the slope (A) and the heave part in the lower part (B), as shown in Fig. 6. The landslide is initiated from the upper part and developed downwards with increasing

displacement. In area A the sliding force is generated and transferred to the lower part, whereas in area B the rock mass are pressed passively. In area A, the slope slides along the weak interlayer, driven by gravity. The deformation of the lower part of the slope is extruded. The sliding surface in area B is almost horizontally, which helps resist the sliding. Once the ground heave in area B develops, the resistant part will be broken by shearing, resulting in landsliding.

The landslide involves an area of 3.72 km^2 that shows superficial cracking and distinct ground displacement. Since Aug 2010, multiple back scarps have appeared on the southern slope. The deformation has been accelerating with

time. By Apr 2013, two back scarps formed at the head of the landslide on the southern slope (Fig. 5). The total length of Back Scarp 1 was approximately 2446 m and that of Back Scarp 2 was approximately 2744 m. Figure 7a shows a number of longitudinal scratches on the scarp. The height of the scarp measured on Nov 9, 2013 was 7.32 m. There was clear ground heave at the foot of the landslide, and dilatancy fissures had also been developed (Fig. 7b). The back scarps at the head of the landslide are located at 280–460 m north of the crown of the landslide on the southern slope, and 60–100 m from two residential areas: the Qiantai and Dongli communities. The east side of the landslide crosses the Shengli development area,

Fig. 7 **a** Photo of the scarp at Back Scarp 1 taken on Nov 9, 2013. **b** Photo of the bulged sector at the foot of the landslide taken on Nov 9, 2013
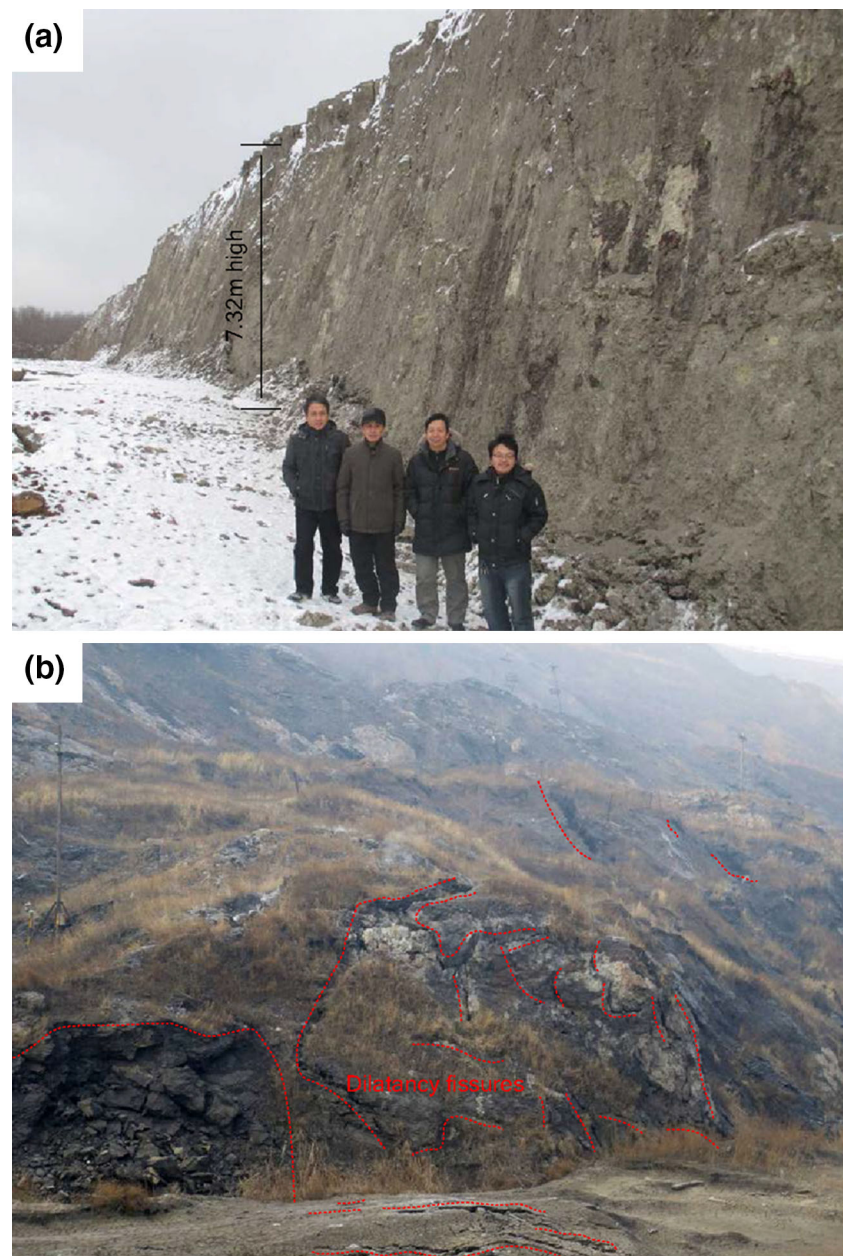
Table 1 Location and elevation of GPS monitoring points

Monitoring points	Data on Feb 25, 2013			Data on Nov 9, 2013		
	X (mE)	Y (mN)	Elevation (m)	X (mE)	Y (mN)	Elevation (m)
GPS0-1	573642	4631346	75	573642	4631346	75
GPS0-2	573728	4631510	90	–	–	–
GPS0-3	573631	4631562	81	–	–	–
GPS0-4	573657	4631716	83	573656.797	4631716.708	82.435
GPS0-5	573590	4631910	8	573589.797	4631910.757	7.591
GPS0-6	573610	4632222	−115	573609.813	4632222.810	−115.253
GPS0-7	573625	4632364	−186	573624.751	4632364.816	−185.752
GPS0-8	573493	4632591	−291	–	–	–
GPS1-1	572703	4630951	67	572703	4630951	67
GPS1-2	572715	4631133	129	–	–	–
GPS1-3	572546	4631165	127	–	–	–
GPS1-4	572667	4631299	210	572666.837	4631299.924	209.446
GPS1-5	572835	4631803	32	572834.860	4631803.998	31.543
GPS1-6	572799	4632133	−111	572798.887	4632134.072	−111.361
GPS1-7	572767	4632364	−216	572766.872	4632365.045	−215.943
GPS1-8	572716	4632607	−290	–	–	–
GPS2-1	574902	4631760	103	574902	4631760	103
GPS2-2	574391	4632350	21	574391	4632350	21
GPS3-1	571669	4631156	112	571669	4631156	112
GPS3-2	571751	4632190	−109	571751	4632190	−109

endangering 4435 lives and 15 businesses. Most of the evidence of surface deformation is situated at the boundary of the landslide in the form of distinct shear surfaces and tension crack. Ground heave at the foot of the landslide has seriously affected the normal open pit mining activities. The collapse of this landslide would pose a serious threat to the safety of the mining operation and the workers in the open pit.

Displacement monitoring and MsTPLP model application

To improve the accuracy of real-time deformation monitoring in the West Open-Pit mine, Global Positioning System (GPS) monitoring is used in the field monitoring. The GPS monitoring network consists of 20 GPS monitoring points, positioned in different parts of the deformation body to monitor the landslide tendency and deformation rate.

There are six GPS deformation monitoring points (GPS0-1, GPS1-1, GPS2-1, GPS2-2, GPS3-1, GPS3-2) outside the landslide risk zone, and 14 monitoring points on the landslide surface, six of which were damaged (GPS0-2, GPS0-3, GPS1-2, and GPS1-3 located near large back scarps at the head of the landslide, and GPS0-8 and GPS1-8 located at the toe of the landslide). The locations of the GPS deformation monitoring points are reported in

Table 1. The monitoring began on Feb 25, 2013; as the deformation increased, the data recording frequency was increased to once a day from Apr 12, 2013. No movement was recorded by GPS0-1, GPS1-1, GPS2-1, GPS2-2, GPS3-1, and GPS3-2. The time series of the cumulative displacements at GPS0-4, GPS0-5, GPS0-6, GPS0-7, GPS1-4, GPS1-5, GPS1-6, and GPS1-7 from Feb 25, 2013 to Nov 9, 2013 and the rainfall versus time for the 2013
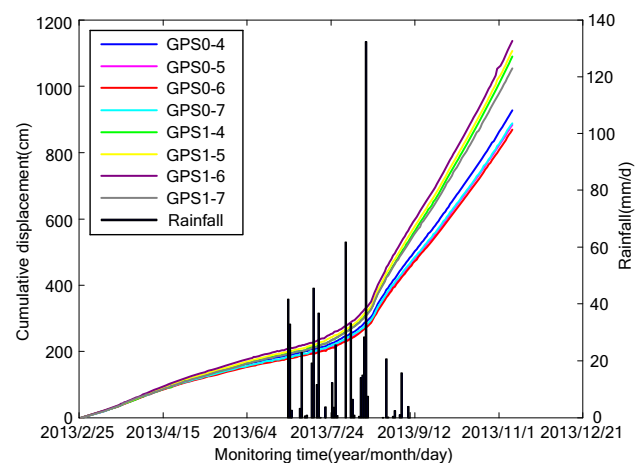

Fig. 8 Cumulative displacements at monitoring points GPS0-4, GPS0-5, GPS0-6, GPS0-7, GPS1-4, GPS1-5, GPS1-6, and GPS1-7 recorded from Feb 25, 2013 to Nov 9, 2013 and the rainfall versus time for the 2013 rainy season
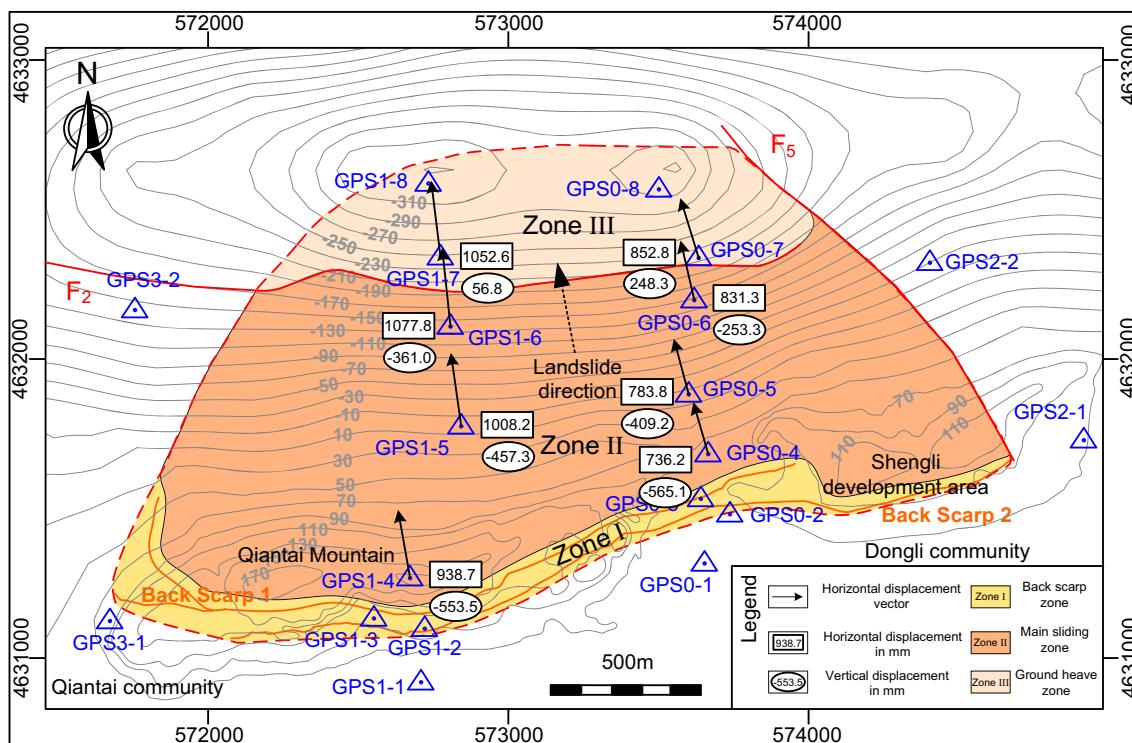
Fig. 9 Map showing the horizontal and vertical displacement recorded from Feb 25, 2013 to Nov 9, 2013 by GPS monitoring. Note that the minus vertical displacement sign represents settlement and the plus vertical displacement sign represents upliftment

rainy season are shown in Fig. 8. We have used these eight GPS monitoring points, which are considered to be representative of different parts of the landslide. The historical displacement of the GPS reflects that the different parts of the landslide mass move synchronically, but with a different displacement rate. The horizontal displacement vectors of GPS1-4, GPS1-5, GPS1-6, and GPS1-7 from Feb 25, 2013 to Nov 9, 2013 were projected onto Section 1-1′. Then the characteristics of sliding failure were indicated by vector sum of vertical and projected horizontal displacements which were obtained from GPS1-4, GPS1-5, GPS1-6, and GPS1-7. As seen from the moving direction given in Fig. 6, area A shows a clear downward displacement, while area B displays a upward displacement. The direction of the surface displacement vectors of the GPS monitoring points on Section 1-1′ and the dip direction of the critical potential sliding surface below the corresponding points in the same direction, correspond well with the dip angle. Based on the monitoring data, the displacement have increased since Aug 2013 and continue to accelerate. Monitoring data analysis showed that by Nov 2013 the horizontal displacement rate of the landslide was 6.3–9.6 cm/day and the vertical displacement rate was between −5.1 and +2.2 cm/day (the minus sign represents settlement and the plus sign represents upliftment). The overall movement of each GPS monitoring point in the

Table 2 Cumulative movements measured by GPS monitoring from Feb 25, 2013 to Nov 9, 2013

Monitoring points	East (mm)	North (mm)	Elevation (mm)
GPS0-4	−202.9	707.7	−565.1
GPS0-5	−202.8	757	−409.2
GPS0-6	−187	810	−253.3
GPS0-7	−249.3	815.6	248.3
GPS1-4	−163	924.4	−553.5
GPS1-5	−140.3	998.4	−457.3
GPS1-6	−112.7	1071.9	−361
GPS1-7	−128.3	1044.8	56.8

horizontal and vertical directions from Feb 25, 2013 to Nov 9, 2013 is presented in Fig. 9 and Table 2. Negative changes in elevation correspond to downward displacement. The landslide is in a continuous deformation state.

When looking at the relationship between the daily rainfall and total cumulative displacements, the landslide deformation appeared to be greatly influenced by maximum daily rainfall, as shown in Fig. 8. The cumulative precipitation at the West Open-Pit mine during Aug 13–18, 2013 was 197.6 mm. Heavy rainfall of 132.3 mm in 11 h were recorded on Aug 16, 2013. Because of the deformation over a long time, multiple tension cracks appeared on the landslide surface. Cracks have been shown to be

preferential infiltration and drainage pathways, and many drainage measures have been damaged. A large amount of rainfall along cracks penetrated into the landslide, the weight of the slip body increased, and the shear strength of the weak interlayer was reduced, which exacerbated the deformation of the landslide. Before Aug 13, the total displacement essentially grew steadily, and the landslide sliding rate was nearly constant (Fig. 8). After Aug 13, the measured displacements showed a rapid and sustained increase, indicating the strong effect of rainfall.

The analysis focuses on the total displacement time series of the monitoring points GPS0-4, GPS0-5, GPS0-6, GPS0-7, GPS1-4, GPS1-5, GPS1-6, and GPS1-7 which reflects the displacement characteristics of the landslide. When the total displacement monitoring data from Nov 3, 2013 to Nov 9, 2013 was analyzed by solution of Eq. 11, the tangential angle of measured displacement curve reached 82°. According to the prediction criteria, the critical condition of the MsTPLP model was reached. The total displacement monitoring data $(t_i, S_i)(i = 1, 2 \ldots, m)$ from Feb 25, 2013 to Nov 9, 2013 of monitoring points GPS0-4, GPS0-5, GPS0-6, GPS0-7, GPS1-4, GPS1-5, GPS1-6, and GPS1-7 as input were successively incorporated into the MsTPLP model. Through the monitoring data fitted by the LM algorithm, the optimal parameters were determined. The predicted displacements were then computed by

solving Eq. 1. To evaluate the performance of the model, displacement comparison between the predicted values and the actual measurement values of total displacements on Nov 9, are shown in Table 3. As shown in Table 3, the predicted values and measured values of total displacements are in very good agreement, and the relative error falls within 6 %. The precision is high enough to satisfy the requirements of deformation prediction of landslides. The results of the forecasted failure time are shown in Table 4.

During the monitoring period, GPS0-4 was the fastest point on Section 0–0′ with the maximum vertical component of measured velocities, but GPS1-6 was the fastest point on Section 1–1′ with the maximum horizontal component of measured ones. The deformation rate of the upper part of Section 0–0′ was greater than that of the middle and lower part. However, the middle part of Section 1–1′ had a greater deformation rate. Considering the deformation characteristics, the vertical deformation of the landslide was divided by geological structure F_2 fault where the upper part showed a clear downwards displacement while the lower part displayed upwards displacement. The displacement pattern is spatially heterogeneous. The landslide was further divided into three deformation zones (Zones I to III) using the landslide deformation monitoring data and the field investigation, as shown in Fig. 9. Located at the upper part of the landslide,

Table 3 Landslide total displacement: a comparison between predicted values and measured values on Nov 9, 2013

Monitoring points	Time (year/month/day)	Measured value (mm)	Predicted value (mm)	Error (mm)	Relative error (%)
GPS0-4	2013/11/9	928.1	974.2	46.1	4.97
GPS0-5	2013/11/9	884.1	927.8	43.7	4.94
GPS0-6	2013/11/9	869.0	912.1	43.1	4.96
GPS0-7	2013/11/9	888.2	932.3	44.1	4.97
GPS1-4	2013/11/9	1089.7	1147.0	57.3	5.26
GPS1-5	2013/11/9	1107.1	1164.7	57.6	5.20
GPS1-6	2013/11/9	1136.7	1194.9	58.2	5.12
GPS1-7	2013/11/9	1054.1	1110.0	55.9	5.30

Table 4 Prediction results of the monitoring network

| Monitoring points	Model parameters				R^2	ARE (%)	Predicted failure time (year/month/day)
	p_0	p_1	p_2	p_3			
GPS0-4	374.098	−5.658	342.915	0.370	0.9876	14.91	2014/3/5
GPS0-5	375.321	1.061	332.428	0.346	0.9874	14.81	2014/3/6
GPS0-6	374.800	0.283	330.636	0.319	0.9873	14.76	2014/3/6
GPS0-7	377.879	0.347	336.090	0.376	0.9878	14.69	2014/3/9
GPS1-4	377.317	−4.366	285.617	0.949	0.9882	16.84	2014/3/8
GPS1-5	379.686	−5.775	306.191	0.942	0.9882	16.53	2014/3/11
GPS1-6	383.031	2.008	327.353	0.975	0.9883	16.17	2014/3/14
GPS1-7	383.980	−1.509	295.987	0.953	0.9881	16.43	2014/3/15

Fig. 10 Failure time prediction of the GPS monitoring point by the MsTPLP model. **a** GPS0-4, GPS0-5, GPS0-6, and GPS0-7 on Section 0–0′. **b** GPS1-4, GPS1-5, GPS1-6, and GPS1-7 on Section 1–1′
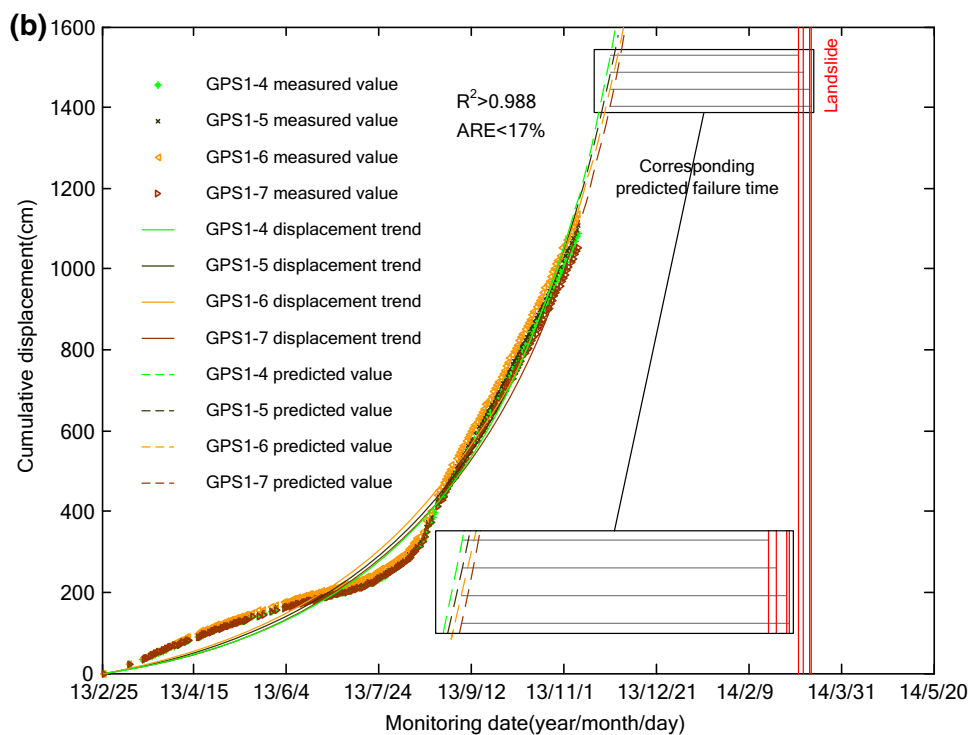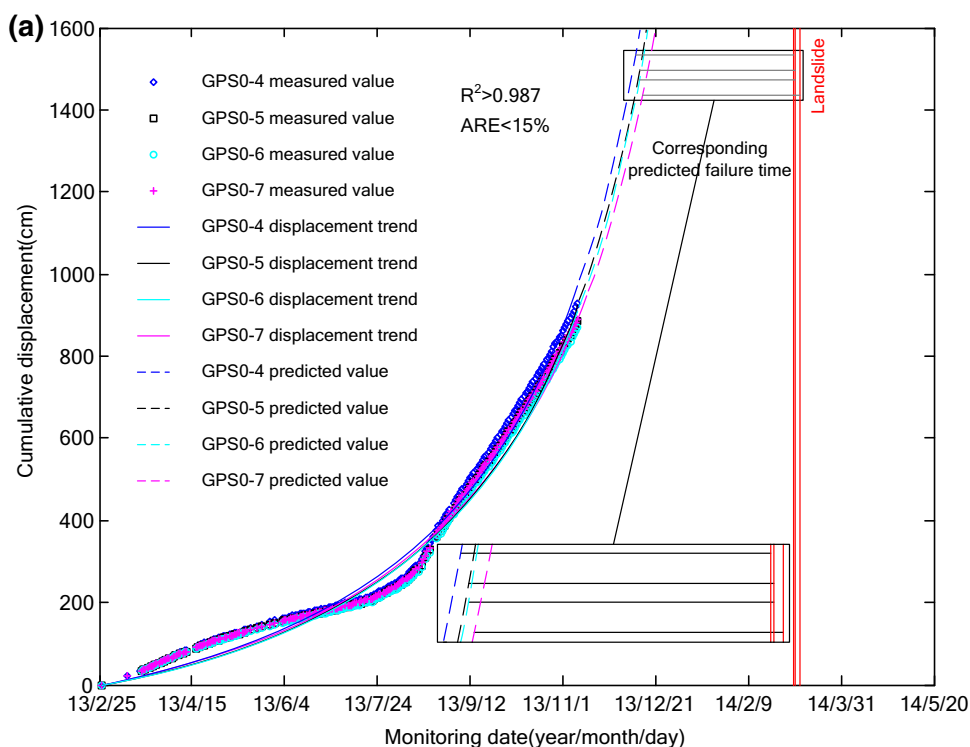
Zone I (Back scarp zone) was approximately 3100 m long and 120 m wide. Large settlement deformations was found in Zone I which formed two back scarps with a total length of approximately 5.2 km. Long depressions parallel to the back scarps can be found in the zone. Many long large cracks appeared at the Shengli development area, and the buildings were tilted or collapsed. Zones II (Main sliding zone) was at the middle part of the landslide, which had a length of approximately 2480 m and a width of 830 m. Also, large deformations are found in Zone II, which was

Fig. 11 Rate averaged over 1 week versus time based on GPS monitoring points (GPS0-4, GPS0-5, GPS0-6, GPS0-7, GPS1-4, GPS1-5, GPS1-6, and GPS1-7) from Mar 11, 2013 to Apr 7, 2014. **a** Horizontal component **b** vertical component
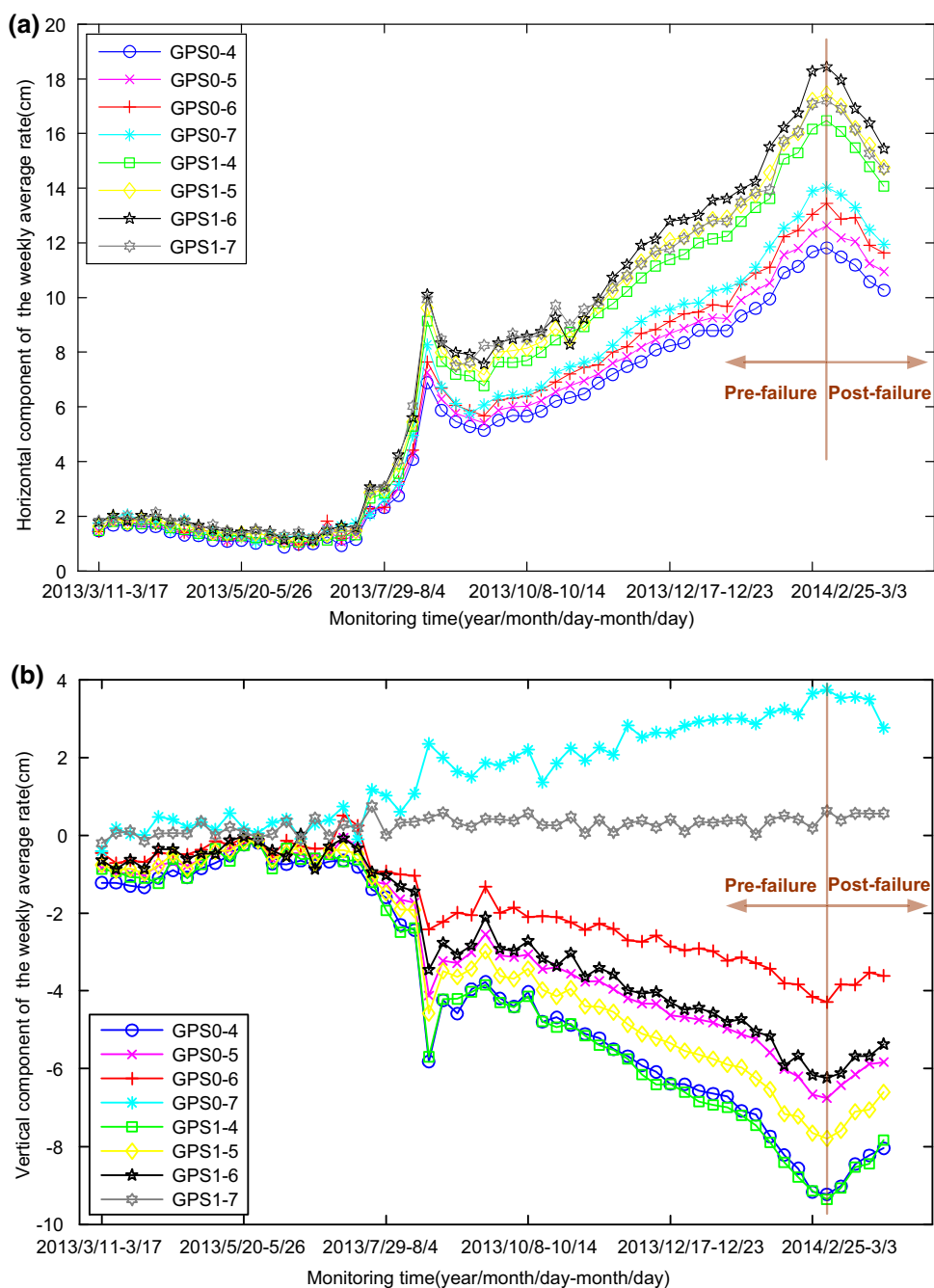
the most active part of the landslide. The deformation of the western side of the landslide was larger than the eastern side. Given that the eastern side of the landslide touches the northern slope, the northern slope has a resistance to landslide. However, the western side still has a certain space to slide. Zone III (Ground heave zone) with a length of approximately 1550 m and a width of 425 m was at the lower part of the landslide, in which an uplifted movement and dilatancy fissures were found. Figure 10 presents a comparison between measured and predicted displacements using the MsTPLP model. It can be observed that the

MsTPLP provides a good matching between the predicted and measured displacements.

The MsTPLP model performs well in terms of R^2 and ARE (R^2 above 0.98 and ARE below 17 %), indicating the acceptability and efficiency of the proposed method in recognizing the landslides with high precision. According to the prediction criteria, a landslide failure occurs when the tangential angle is 90°, that is, the gradient of the accumulated displacement tends to infinity (i.e., $\Delta t \rightarrow 0$ and $\Delta S \rightarrow \infty$). In our study, using eight different measuring positions, the displacement versus time curve varies,

and the predicted landslide failure time is not consistent. The prediction results of monitoring points GPS0-7 and GPS1-7 reflect predicted failure time and displacement trend in Zone III. The prediction results of the monitoring points GPS0-4, GPS0-5, GPS0-6, GPS1-4, GPS1-5, and GPS1-6 reflect the predicted failure time in Zone II, which is the most active zone. The data of GPS0-4 and GPS1-6 represent the maximum deformation rate in eastern side and western side of the Zone II, respectively, which provide the most active part description of entire landslide movement. The ARE value in the prediction results of the monitoring point GPS0-4 was lower than the GPS1-6, which indicates the accuracy of the prediction result of GPS0-4 is higher. That's the reason why the predicted failure time of GPS0-4 is selected as the final prediction value. The forecast results for the landslide show that the estimated failure time is Mar 5, 2014.

Combined with the displacement monitoring data, the horizontal and vertical rate components averaged over 1 week from the GPS monitoring points (GPS0-4, GPS0-5, GPS0-6, GPS0-7, GPS1-4, GPS1-5, GPS1-6, and GPS1-7) from Mar 11, 2013 to Apr 7, 2014 are shown in Fig. 11a, b, respectively. The horizontal and vertical components of the weekly average rate reached a maximum on the week of Mar 4–10, 2014. According to records, the maximum daily displacement rate on that week was on Mar 9, 2014. On Mar 9, 2014, the horizontal displacement rate was 12.4–20.8 cm/day, the vertical displacement rate was −10.6 to +5.6 cm/day (the minus sign represents downward sliding and the plus sign represents upward uplift). Note that the rate on Mar 9, 2014 is the peak rate. According to failure time analysis described in the "Model evaluation" section, the landslide on the southern slope of the West Open-Pit mine occurred on Mar 9, 2014. After March 10, the weekly average rate gradually decreased, but the landslide displacement still increased throughout the monitoring period, and the landslide mass gradually tended to stabilize. The weekly average landslide rate is divided into pre-failure and post-failure regions according to the peak rate. The deformation movements after Mar 10, 2014 are post-failure movements.

In conclusion, the landslide failure time on the southern slope of the West Open-Pit mine and the predicted failure time are very close. The results indicated that the model can be applicable to the prediction of landslides subject to creep deformation.

Conclusions and discussion

The following conclusions were drawn from our study:

1. In accordance with the MsTPLP model curve characteristics, the deformation features of the landslide on the southern slope of the West Open-Pit Mine are creep slopes. The tangential angle did not reach 82° until the monitoring data on Nov 9, 2013. The displacement monitoring data from Feb 25, 2013 to Nov 9, 2013 was incorporated into the MsTPLP model. The optimal model parameters of the MsTPLP model are determined by the LM method. The MsTPLP model performs well in fitting the displacement series in terms of R^2 and ARE (R^2 above 0.98 and ARE below 17 %). The prediction results of the landslide on the southern slope of the West Open-Pit mine show the predictive failure time is Mar 5, 2014. And the landslide on the southern slope of the West Open-Pit mine occurred on Mar 9, 2014. The predicted failure time and the actual failure time were very close, indicating that the MsTPLP model successfully predicted the landslide.

2. The MsTPLP model appears to be a feasible and capable landslide prediction method. Based on the Levenberg–Marquardt algorithm, using deformation monitoring data, the prediction displacement versus time curve shape is constantly adjusted to adapt to the evolution process of the landslide. When the critical condition is reached, the prediction results achieve high accuracy with acceptable average relative errors. The MsTPLP model provides a useful tool for landslide prevention and mitigation. However, the MsTPLP model is in calibration and validation periods. Further analysis is needed to explore the temporal variability of prediction and a landslide early warning system. The MsTPLP model should be tested on other cases to assess its generalization and predictive power.

References

Agliardi F, Crosta GB, Frattini P (2010) Forecasting the failure of large landslides for early warning: issues and directions. In Landslide Monitoring Technologies and Early Warning Systems-Current Research and Perspectives for the Future. Vienna: Geological Survey of Austria 82:48–49

Cai Z, Xu W, Meng Y et al (2015) Prediction of landslide displacement based on GA-LSSVM with multiple factors. Bull Eng Geol Environ. doi:10.1007/s10064-015-0804-z

Chen H, Zeng Z, Tang H (2015) Landslide deformation prediction based on recurrent neural network. Neural Process Lett 41(2):169–178

China Geological Environmental Monitoring Institute (2014) Chinese geological disasters Bulletin 2013. China geological environment information site. http://www.cigem.gov.cn. Accessed 10 June 2014

Crosta GB, Agliardi F (2003) Failure forecast for large rock slides by surface displacement measurements. Can Geotech J 40(1):176–191

Du J, Yin K, Lacasse S (2013) Displacement prediction in colluvial landslides, three Gorges reservoir, China. Landslides 10(2):203–218

Federico A, Popescu M, Elia G et al (2012) Prediction of time to slope failure: a general framework. Environ Earth Sci 66(1):245–256

Griffiths JS (1999) Proving the occurrence and cause of a landslide in a legal context. Bull Eng Geol Environ 58(1):75–85

Haefeli R (1953) Creep problems in soils, snow and ice. In: Proceedings of 3rd international conference on soil mechanics and foundation engineering 3: 238–251

Huang RQ (2012) Mechanisms of large-scale landslides in China. Bull Eng Geol Environ 71(1):161–170

Huang RQ, Wang ST, Zhang ZY et al (2002) Shallow earth crust dynamics process and engineering environment research in Western China. Sichuan University Press, Chengdu

Hungr O, Leroueil S, Picarelli L (2014) The Varnes classification of landslide types, an update. Landslides 11(2):167–194

Johnson EA (1990) Geology of the Fushun coalfield, Liaoning province, People's Republic of China. Int J Coal Geol 14(3):217–236

Leroueil S, Locat J, Vaunat J, Picarelli L, Lee H, Faure R (1996) Geotechnical characterization of slope movements. In: Senneset K (ed) Landslides. Balkema, Rotterdam, pp 53–74

Levenberg K (1944) A method for the solution of certain non-linear problems in least squares. Q Appl Math 2(2):164–168

Li XZ, Kong JM, Wang ZY (2012) Landslide displacement prediction based on combining method with optimal weight. Nat Hazards 61(2):635–646

Lian C, Zeng ZG, Yao W et al (2015) Multiple neural networks switched prediction for landslide displacement. Eng Geol 186:91–99

Liu Z, Shao J, Xu W et al (2014) Comparison on landslide nonlinear displacement analysis and prediction with computational intelligence approaches. Landslides 11(5):889–896

Lourakis MIA (2005) A brief description of the Levenberg-Marquardt algorithm implemented by levmar. Found Res Technol 4:1–6

Marquardt DW (1963) An algorithm for the least-squares estimation of nonlinear parameters. J Soc Ind Appl Math 11(2):431–441

Mazzanti P, Bozzano F, Cipriani I et al (2015) New insights into the temporal prediction of landslides by a terrestrial SAR interferometry monitoring case study. Landslides 12(1):55–68

Nie L, Zhang M, Shen SW (2013) Geological Environment and Slope Failure Mode in Southeast Region of Jilin Province, China. Disaster Adv 6(2):73–80

Nie L, Li ZC, Zhang M, Xu LN (2015) Deformation characteristics and mechanism of the landslide in West Open-Pit Mine, Fushun, China. Arab J Geosci 8(7):4457–4468

Qin SQ, Jiao JJ, Wang SJ (2001) The predictable time scale of landslides. Bull Eng Geol Environ 59(4):307–312

Radbruch-Hall DH, Varnes DJ (1976) Landslides—cause and effect. Bull Eng Geol Environ 13(1):205–216

Rose ND, Hungr O (2007) Forecasting potential slope failure in open pit mines–contingency planning and remediation. Int J Rock Mech Min 44:308–320

Saito M (1969) Forecasting time of slope failure by tertiary creep. In: Proceedings of the 7th International Conference on Soil Mechanics and Foundation Engineering. Mexico: Sociedad Mexicana de Mecanicade Suelos, A.C.,pp. 677–683

Sättele M, Krautblatter M, Bründl M et al (2015) Forecasting rock slope failure: how reliable and effective are warning systems? Landslides. doi:10.1007/s10346-015-0605-2

Sidle RC, Ochiai H (2006) Landslides: processes, prediction, and land use. American Geophysical Union, Washington

Skempton AW, Hutchinson JN (1969) Stability of natural slopes and embankment foundations. Proceedings, 7th International conference of soil mechanics and foundation engineering. State of the Art volume, Mexico, pp 291–340

Terzaghi K (1950) Mechanism of landslides (Berkey Volume). Geological Society of America, New York, pp 83–124

Wang RX, Nie L (2010) Landslide prediction in Fushun West Open Pit mine area with quadratic curve exponential smoothing method. In: 18th International Conference, Beijing, China doi: 10.1109/GEOINFORMATICS.2010.5567832

Wu C, Yang Q, Zhu Z, Liu G, Li X (2000) Thermodynamic analysis and simulation of coal metamorphism in the Fushun Basin, China. Int J Coal Geol 44(2):149–168

Xu Q, Zeng YP (2009) Research on acceleration variation characteristics of creep landslide and early-warning prediction indicator of critical sliding. Chin J Rock Mech Eng 28(6):1009–1106 (in Chinese)

Xu Q, Tang MG, Xu KX (2008) Research on space-time evolution laws and early warning-prediction of landslides. Chin J Rock Mech Eng 27(6):1104–1112 (in Chinese)

Xu Q, Yuan Y, Zeng YP et al (2011) Some new pre-warning criteria for creep slope failure. Sci China Technol Sc 54(1):210–220

Zhang SX (2009) Fushun Formation. In: Geological formation names of China (1866–2000), Beijing, pp 302–361

Zhang M, Nie L, Xu Y et al (2015) A thrust load-caused landslide triggered by excavation of the slope toe: a case study of the Chaancun Landslide in Dalian City, China. Arab J Geosci 8(9):6555–6565

Zhou JJ, Chen L, Fu ZL et al (2011) Study on geological hazards and countermeasures in Fushun mining area. Appl Mech Mater 71:4839–4843